PCCP

Ordered Mesoporous Ferrosilicate Materials with Highly Dispersed Iron Oxide Nanoparticles and Investigation of Their Unique Magnetic Property

Journal:	*Physical Chemistry Chemical Physics*
Manuscript ID:	CP-COM-07-2014-003216.R1
Article Type:	Communication
Date Submitted by the Author:	30-Aug-2014

Complete List of Authors:	Pavuluri, Srinivasu; Indian Institute of Chemical Technology (IICT), Inorganic and Physical Chemistry Division Suresh, Koppoju; International Advanced Research Centre for Powder Metallurgy and New Materials, Datta, Gopal; Defence Institute of Advanced Technology, Department of Materials Engineering Abhayankar, Ashutosh; Defence Institute of Advanced Technology, Rao, Pinjala; National Institute of Technology, Department of Chemistry Lakshmi Kantam, M; Indian Institute of Chemical Technology, Inorganic Nad Physical Chemistry Division Bhargava, Suresh; RMIT University, School of Applied Science Tang, Jing; National Institute for Materials Science, Yamauchi, Yusuke; National Institute for Materials Science, WPI Center for MANA

SCHOLARONE™
Manuscripts

Cite this: DOI: 10.1039/c0xx00000x

www.rsc.org/xxxxxx

ARTICLE TYPE

Ordered Mesoporous Ferrosilicate Materials with Highly Dispersed Iron Oxide Nanoparticles and Investigation of Their Unique Magnetic Property

Pavuluri Srinivasu,[1]* Koppoju Suresh,[2] Gopal Datta,[3] Ashutosh C. Abhayankar,[3] Pinjala Nageswara Rao,[4] Mannepalli Lakshmi Kantam,[1] Suresh K. Bhargava,[5] Jing Tang,[6] and Yusuke Yamauchi[6]*

Received (in XXX, XXX) XthXXXXXXXXX 20XX, Accepted Xth XXXXXXXXX 20XX
DOI: 10.1039/b000000x

Ordered mesoporous ferrosilicate materials with highly dispersed iron oxide nanoparticles are directly synthesized through hydrothermal approach under acidic conditions. The obtained samples possess high surface area (up to 1236 $m^2 \cdot g^{-1}$) and large pore volume (up to 1.1 $cm^3 \cdot g^{-1}$). By changing the amount of iron content, the magnetic properties can be tuned.

In the past decade, a wide range of mesoporous materials have already been devoted to create a large number of functional materials, particularly in the areas of catalysis, adsorption, fuel cells, solar cells, and biomaterials.[1] For these applications, textural properties such as high surface area and large pore volume are very critical. Much effort is being made to enhance the properties of mesoporous materials by using either a cationic or an anionic or a neutral surfactant as a structure directing agent. Thus, two (2D) and three dimensional (3D) mesoporous materials (*e.g.*, MCM-41, MCM-48, HMS, SBA-1, SBA-15, and AMS) have been synthesized.[2] The potential applications of mesoporous silica materials especially for drug deliver and magnetic systems often require well-designed mesoporous architectures with controlled textural properties.[3]

Recently, magnetic nanomaterials have emerged as a new class of promising materials for potential applications in data storage, magnetic carriers for drug delivery, electronic and biomedical devices.[4] In addition, porous magnetic structures are one of the important multi-functional materials that have been attracted great attention of physicists, chemists, and materials scientists.[5] In particular, porous inorganic architectures, hybrid organic/inorganic compounds or metal-organic compounds with high porosity have capability of hosting many guests for applications. However, many of these applications require highly dispersed iron oxide nanoparticles as they demonstrate remarkable magnetic properties. The creation of ordered porous structure together with tunable magnetic properties is very difficult by using traditional methods.

Most of the traditional methods, such as thermal decomposition of organometallic compounds, sonochemistry, and hot injection method devoted for the production of iron oxide nanoparticles still suffer from complicated synthesis procedures. Therefore, it is a great challenge to develop highly imperative synthetic route for fabrication of mesoporous magnetic materials with highly dispersed iron oxide particles in a single approach.

In this synthetic protocol, we demonstrate a direct hydrothermal synthesis method to prepare mesoporous ferrosilicate materials (PS-1) with highly dispersed iron oxide nanoparticles in a single approach using Brij 76 polymer under acidic conditions. Interesting point of this method is that controlling the textural properties, such as surface areas, pore volumes, and pore diameters together with their magnetic properties, without the need of distinct addition of iron precursors, simply by changing the iron content in the porous matrix in a single approach (**Fig. 1**). The obtained products were denoted as PS-1(*x*), where *x* represents Si/Fe mole ratios. For comparison, mesoporous silica material (MPS) without iron content was also prepared.

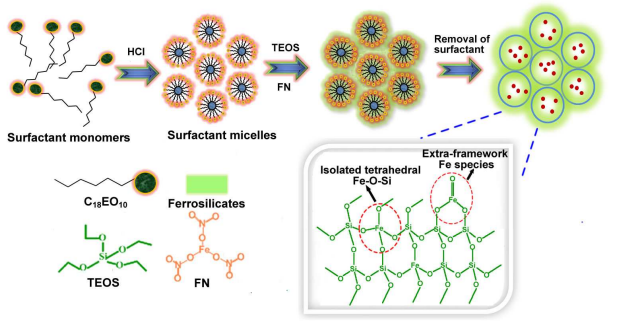

Fig. 1 Schematic representation of preparation of mesoporous ferrosilicate materials with highly dispersed iron oxide nanoparticles by a facile hydrothermal synthesis method.

The structural characterization of PS-1 materials prepared at different Si/Fe mole ratios are investigated using small-angle X-ray scattering (SAXS). The SAXS patterns of PS-1 materials are shown in **Fig. 2a**, which determine the degree of mesostructural order, average lattice parameter values, and possible mesostructures. All the materials exhibit main characteristic planes of (10), (11) and (20), showing well-resolved reflections representing a 2D hexagonal mesoporous structure, similar to mesoporous silica materials described by Zhao *et al.*[6] The intensity of the observed SAXS peaks are well maintained even after the ferrosilicate formation, which is indicative of a high degree of mesostructural regularity. The peak positions were

shifted towards lower *q*-region with increasing the iron content. The pore-to-pore distance calculated by SAXS data of mesoporous silica (MPS) prepared under similar experimental conditions is 5.91 nm, and this value increases up to 6.52 nm of PS-1(22) material with increasing iron content (**Table 1**).

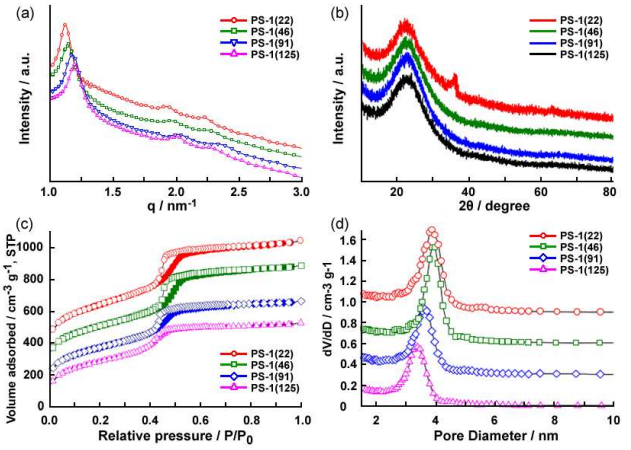

Fig. 2 (a) Small-angle X-ray scattering (SAXS) patterns, (b) wide-angle XRD patterns of PS-1 materials with different Si/Fe mole ratios (PS-1(125), PS-1(91), PS-1(46), and PS-1(22)), (c) Nitrogen adsorption-desorption isotherms of PS-1 materials, and (d) the corresponding pore size distributions. In Figure (b), the peak located at 2θ = around 36 (degree) corresponds to the formation of crystalline Fe oxide nanoparticles inside the mesopores.

Table 1. Summary of pore-to-pore distances, surface areas, pore volumes, and pore sizes of PS-1 materials with different Si/Fe mole ratios (PS-1(125), PS-1(91), PS-1(46), and PS-1(22)) and MPS materials.

Sample	Pore-to-pore distance (nm)	Surface area ($m^2 \cdot g^{-1}$)	Pore Volume ($cm^3 \cdot g^{-1}$)	Pore size (nm)
PS-1(22)	6.52	1236	1.1	3.9
PS-1(46)	6.49	1116	1.0	3.9
PS-1(91)	6.34	1077	0.89	3.5
PS-1(125)	6.22	1028	0.80	3.4
MPS	5.91	890.0	0.64	3.0

The elemental compositions of calcined PS-1 materials were examined by inductive coupled plasma (ICP) and energy dispersive X-ray spectroscopy (EDS). The EDS data clearly shows only Fe, Si and O element peaks (**Fig. S1**), demonstrating that polymeric template is completely removed during the calcination process. Elemental compositions obtained from EDS data is in agreement with ICP data. The corresponding elemental mapping of the PS-1(22) indicates the uniform distribution of Fe atoms throughout the material. The porosity of PS-1 and MPS materials without Fe content was measured by nitrogen adsorption-desorption isotherms, as shown in **Fig. 2c** and **S2**. All the materials possess classical of type IV isotherm with steep capillary condensation steps occurring at relative pressures P/P_0 of 0.4-0.6, characteristic of mesoporous materials. The textural properties of PS-1 and MPS materials are summarized in **Table 1**. With the increase of iron content, the specific surface areas and total pore volumes greatly are increased from 1028 $m^2 \cdot g^{-1}$ and 0.8 $cm^3 \cdot g^{-1}$ for PS-1(125) to 1236 $m^2 \cdot g^{-1}$ and 1.1 $cm^3 \cdot g^{-1}$ for PS-1(22) respectively. These values are higher than that of MPS synthesized under similar conditions. A significant increase in specific surface area with increasing iron content is mainly due to the improvement in structure order of rigid PS-1 materials, which is clearly reflected in SAXS patterns of PS-1 materials. Furthermore, it is interesting to note that the capillary condensation step shifts to higher relative pressures, which directly reveals that the mesopore diameters (**Fig. 2d**) significantly increases from 3.4 to 3.9 nm with increasing iron content in mesoporous framework. The results are in quite good agreement with the data obtained from SAXS data.

To investigate the formation of iron oxide nanoparticles in the mesochannels, PS-1(22) materials were characterized by transmission electron microscopy (TEM). Highly magnified TEM image of PS-1(22) and the particle size distribution histogram of the deposited iron oxide nanoparticles are shown in **Fig. 3**. The mesoporosity of the PS-1 materials with linear array of mesochannel is clearly confirmed. The iron oxide nanoparticles are well dispersed on porous channels. It is clearly confirmed that an efficient formation of isolated iron oxide nanoparticles with particle sizes of 5-6 nm under mesoporous ferrosilicate growth conditions. It is found that the mesostructural order is well maintained even after incorporation of high amount of iron into the mesoporous channels. Except for PS-1(22), other samples with lower iron content do not show any diffraction peaks (**Fig. 2b**), implying that no crystalline nanoparticles are not deposited (*i.e.*, all the iron species are incorporated in the silicate framework.).

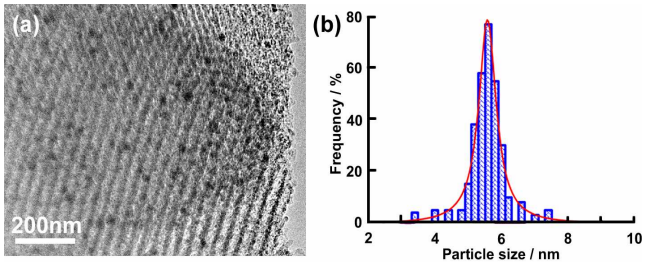

Fig. 3 (a) TEM image of PS-1(22) and (b) the particle size distribution histogram of the deposited iron oxide nanoparticles of PS-1(22) material.

UV-Vis diffuse reflectance spectroscopy was employed in order to prove charge-transfer bands and coordination number of iron species in PS-1 materials. The spectra of calcined PS-1 materials with different Si/Fe ratios show a very intense band at 240-270 nm, which is usually taken as clear evidence for charge-transfer transition between iron and oxygen in the Fe-O-Si framework.[7a] Interestingly, PS-1(22) material shows broad band arising at 350-450 nm is assigned to oligonuclear Fe species in extra-framework position.[7b] The coordination state of Fe species in MPS framework is considerably affected by changing the iron content in the PS-1materials.

By treatment with HF solution[8] the silicate frameworks are dissolved and Fe_3O_4 crystalline nanoparticles are predominately formed. The obtained sample is denoted as HF-treated PS-1(22). The wide-angle XRD pattern for HF-treated PS-1(22) is shown in **Fig. S3**. In order to understand the magnetic properties, zero filed

This journal is © The Royal Society of Chemistry [year]

cooling (ZFC) and field cooling (FC) magnetization curves were measured at DC magnetic field of 50 Oe for HF-treated PS-1(22) and PS-1(22) samples from 10 K to 350 K (**Fig. 4a-b**). Irreversibility in ZFC-FC magnetization is very similar in both HF-treated PS-1(22) and PS-1(22), due to presence of superparamagnetic relaxation of the nanoparticles.[9] Moreover, ZFC magnetization do not exhibit peak in both the samples reveals that blocking temperature, T_B > 350 K in PS-1(22) and HF-treated PS-1(22). However, the close scrutiny of the data reveals value of magnetization at 50 Oe in case of HF-treated PS-1(22) is two orders of magnitude higher than PS-1(22). This reduction in magnetization is attributed to the formation of mesoporous magnetically diluted ferrosilicate formation where iron oxide particles are well separated in non-framework sites in the case of PS-1(22).

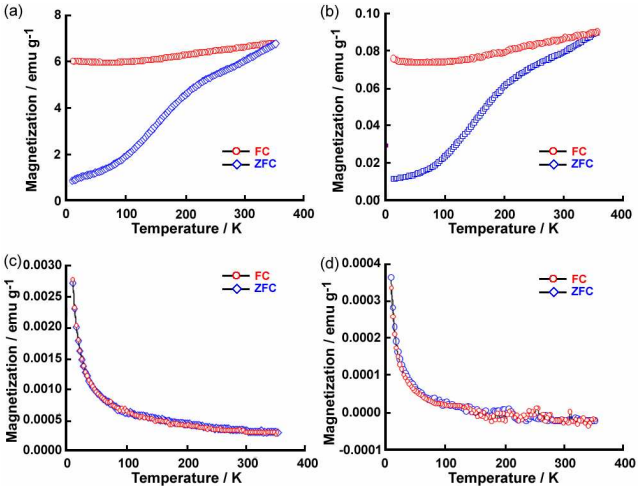

Fig. 4 FC and ZFC curves of (a) HF-treated PS-1(22), (b) PS-1(22), (c) PS-1(46), and (d) PS-1(91), respectively.

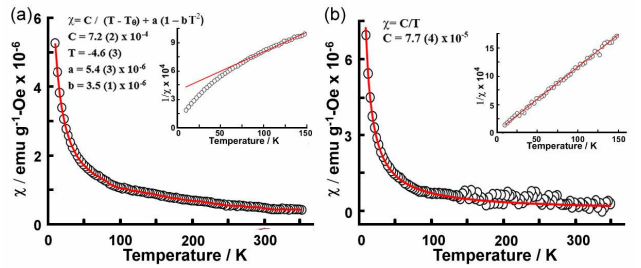

Fig. 5 DC magnetic susceptibility (χ) as a function of temperature (*T*) for (a) PS-1(46) and (b) PS-1(91), respectively. Plots of 1/χ(*T*) *vs. T* plots at low temperatures are shown as inset.

ZFC-FC curves of PS-1(46) and PS-1(91) materials show complete reversibility and paramagnetic behavior down to T = 10 K, as shown in **Fig. 4c-d**. Both PS-1(46) and PS-1(91) samples exhibit concave upward curvature of $M(T)$ reminiscent of paramagnetic the Curie law. It is important to note that magnitude of $M(T)$ is one order lower in case of PS-1(91) as compared to PS-1(46) due to further dilution of iron content in the framework. In order to investigate the magnetism of PS-1(46) and PS-1(91), DC susceptibility is plotted as a function of temperature, $\chi(T)$ (**Fig. 5**) and analyzed using the Curie/Curie-Weiss law. In case of PS-1(91), the experimental data fits well with paramagnetic Curie law with Curie constant, C = 7.7(4)×10^{-5}, which yields μ_{eff} = 0.27(1) considering ferrosilicates ((FeSi)O_2) as a formula unit. (**Fig. 5b**) Such low moments show that superparamgnetic iron oxide nanoparticles are absent at non-framework site, which is in good agreement with earlier reports.[10] As shown in inset of **Fig. 5b**, $1/\chi(T)$ vs. T curve passes through the origin, which reveals that PS-1(91) exhibits paramagnetic behavior down to 9 K consistent with Curie's law.[11] However, $\chi(T)$ of PS-1(46) could not be accounted by using either Curie or Curie-Weiss law due to complex magnetic correlations, although non-linear least square fits yields lower chi-sq value for the latter than the former. In addition, the $\chi(T)$ data of PS-1(46), is then fitted by modified Curie-Weiss law with exchange-enhanced Pauli contributions (χ_{EP})[12] represented by the following equation,

$$\chi(T) = \chi_{CW}(T) + \chi_{EP}(T) = C/(T-T_\theta) + a\,(1 - bT^2)$$

where C denotes Curie constant, T_θ denotes paramagnetic Curie temperature, a denotes exchange-enhanced Pauli susceptibility, χ_{EP} at T = 0 K, and b represents contribution from density of states at the Fermi level.

As shown in **Fig. 5a**, the free fitting parameters used in these fits yield the values for C= 7.2(2)×10^{-4}, T_θ= -4.6(3), a= 5.4(3)×10^{-6}, and b= 3.5(1)×10^{-6}, respectively. Very small negative values of T_θ indicate the presence of antiferromagnetic correlations that are just building up in PS-1(46). Moreover, the values of a and b obtained in PS-1(46) from the fittings are very small (10^{-6}) compared to exchange-enhanced Pauli contribution reported in the literature (10^{-4}).[13] Interestingly, $1/\chi(T)$ vs. T plot in **Fig. 5a** (inset) clearly confirms the existence of antiferromagnetic correlations for PS-1(46) material at low temperatures. The calculated magnetic moment in case of PS-1(46) is μ_{eff} = 0.82(1), which is around three times larger than PS-1(91). Thus, it can be concluded that in mesoporous framework of ferrosilicates the magnetic properties of PS-1 materials can be tuned by simply controlling the iron content in porous structure.

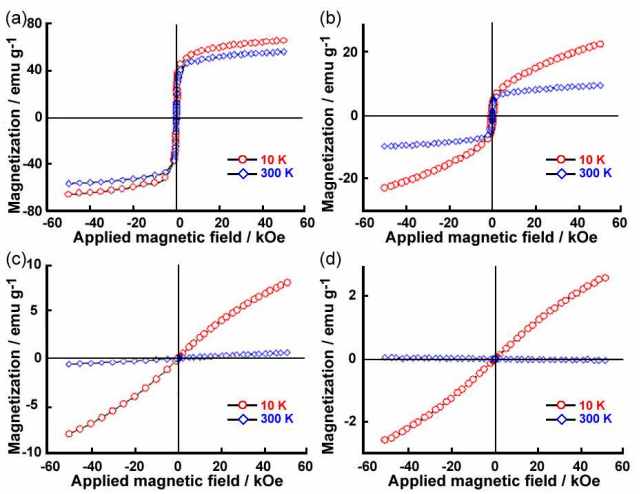

Fig. 6 Magnetic hysteresis loops of (a) HF-treated PS-1(22), (b) PS-1(22), (c) PS-1(46) and (d) PS-1(91), respectively.

To further investigate the magnetic properties, magnetic hysteresis loops were measured at 10 K and 300 K in the magnetic fields of 5T for all the samples (**Fig. 6**). Saturation magnetization (M_s) value of HF-treated PS-1(22) at 10 K was 65 emu·g^{-1}. In the case of PS-1(22), the M_s value was reduced to 22 emu·g^{-1} at 10 K, and it was far from saturation, due to the presence of distinct impurity phase (antiferromagnetic α-Fe_2O_3) (**Fig. 6a**). However, PS-1(22) exhibits sharp magnetic saturation at low fields at 300 K as shown in **Fig 6b**. This behavior is attributed to weakening of antiferromagnetic interactions (of

distinct impurity phase) and unfreezing of superparamagnetic γ-Fe_2O_3 or Fe_3O_4 particles at 300 K, which can be aligned easily at lower magnetic fields.[14] In case of PS-1(46) and PS-1(91) paramagnetic behavior down to 10 K is reminiscent from the M *vs.* H loops displayed from **Fig. 6c-d**. At 300 K, PS-1(91) displays weak diamagnetic response, whereas PS-1(46) is paramagnetic.

In summary, we demonstrated a facile approach for synthesis of mesoporous ferrosilicates with highly dispersed iron oxide nanoparticles and tunable textural properties. Nitrogen adsorption isotherms reveal that the surface areas of PS-1 materials significantly increase with increasing the iron content, meanwhile the pore diameters also increase from 3.4 nm to 3.9 nm. Moreover, the magnetic properties of PS-1 materials can be tuned simply by adjustment of iron content in mesoporous matrix. Consequently, the present strategy will be helpful for further design of various mesoporous materials with unique magnetic properties.

Notes and references

1 Inorganic and Physical Chemistry Division, CSIR-Indian Institute of Chemical Technology, Hyderabad- 500007, India, E-mail: pavuluri.srini@iict.res.in

2 International Advanced Research Centre for Powder Metallurgy and New Materials, Hyderabad-500005, India.

3 Department of Materials Engineering, Defence Institute of Advanced Technology, Girinagar, Pune 411025, India

4 Department of Chemistry, National Institute of Technology, Warangal 506004, India

5 School of Applied Sciences, RMIT University, Melbourne, Victoria 3001, Australia.

6 World Premier International (WPI) Research Center for Materials Nanoarchitectonics, National Institute for Materials Science (NIMS), 1-1 Namiki, Tsukuba, Ibaraki 305-0044, Japan. E-mail: Yamauchi.Yusuke@nims.go.jp

† Electronic Supplementary Information (ESI) available. See DOI: 10.1039/b000000x/

1 (a) J. Lee, S. Yoon, T. Hyeon, S. Oh, K. B. Kim, *Chem. Commun.*, 1999, **21**, 2177; (b) J. H. Clark, *Acc. Chem. Res.*, 2002, **35**, 791; (c) F. Goettmann, A. Moores, C. Boissiere, P. Le Floch, C. Sanchez, *Small*, 2005, **1**, 636; (d) M. Zukalova, A. Zukal, L. Kavan, M. K. Nazeeruddin, P. Liska, M. Gratzel, *Nano Lett.*, 2005, **5**, 1789; (e) Y. Fang, D. Gu, Y. Zou, Z. Wu, F. Li, R. Che, Y. Deng, B. Tu, D. Zhao, *Angew. Chem. Int. Ed.,* 2010, **49**, 7987; (f) P. Hartmann, D. K. Lee, B. M. Smarsly, J. Janek, *ACS Nano*, 2010, **4**, 3147; (g) K. Ariga, A. Vinu, Y. Yamauchi, Q. Ji, J. P. Hill, *Bull. Chem. Soc. Jpn.*, 2012, **85**, 1. (h) Y. Yamauchi, *J. Ceram. Soc. Jpn.*, 2013, **121**, 831.

2 (a) C. T. Kresge, M. E. Leonowicz, W. J. Roth, J. C. Vartuli, J. S. Beck, *Nature,* 1992, **359**, 710; (b) P. T. Tanev, M. Chibwe, T. J. Pinnavaia, *Nature,* 1994, **368**, 321; (c) Q. Huo, D. I. Margolese, G. D. Stucky, *Chem. Mater.*, 1996, **8**, 1147; (d) D. Zhao, J. Feng, Q. Huo, N. Melosh, G. H. Fredrickson, B. F. Chmelka, G. D. Stucky, *Chem. Mater.,* 1998, 279, 548; (e) R. Ryoo, S. H. Joo, J. M. Kim, *J. Phys. Chem. B* 1999, **103**, 7435; (f) S. Che, Z. Liu, T. Ohsuna, K. Sakamoto, O. Terasaki, T. Tatsumi, *Nature,* 2004, **429**, 281.

3 (a) J. Kim, J. E. Lee, J. Lee, J. H. Yu, B. C. Kim, K. An, Y. Hwang, C. H. Shin, J. G. Park, J. Kim, T. Hyeon, *J. Am. Chem. Soc.,* 2006, **128**, 688; (b) E. Kockrick, P. Krawiec, W. Schnelle, D. Geiger, F. M. Schappacher, R. Pottgen, S. Kaskel, *Adv. Mater.,* 2007, **19**, 3021; (c) W. R. Zhao, H. G. Chen, Y. S. Li, L. Li, M. D. Lang, J. L. Shi, *Adv. Funct. Mater.,* 2008, **18**, 2780; (d) M. Liong, S. Angelos, E. Choi, K. Patel, J. F. Stoddart, J. I. Zink, *J. Mater. Chem.,* 2009, **19**, 6251; (e) Y. Chen, H. Chen, S. Zhang, F. Chen, L. Zhang, J. Zhang, M. Zhu, H. Wu, L. Guo, J. Feng, J. Shi, *Adv. Funct. Mater.,* 2011, **21**, 270.

4 (a) C. Xu, K. Xu, H. Gu, R. Zheng, H. Liu, X. Zhang, Z. Guo, B. Xu, *J. Am. Chem. Soc.,* 2004, **126**, 9938; (b) V. Salguirino-Maceira, M. A. Correa-Duarte, M. Spasova, L. M. Liz-Marzan, M. Farle, *Adv. Funct. Mater.,* 2006, **16**, 509; (c) J. Bachmann, J. Jing, M. Knez, S. Barth, H. Shen, S. Mathur, U. Gosele, K. Nielesch, *J. Am. Chem. Soc.,* 2007, **129**, 9554; (d) S. G. Kwon, Y. Piao, J. Park, S. Angappane, Y. Jo, N. M. Hwang, J. G. Park, T. Hyeon, *J. Am. Chem. Soc.,* 2007, **129**, 12571; (e) A. H. Lu, E. L. Salabas, F. Schüth, *Angew. Chem. Int. Ed.,* 2007, **119**, 1242.

5 (a) J. F. Long, M. S. Logan, C. P. Rhodes, E. E. Carpenter, R. M. Stroud, D. R. Rolison, *J. Am. Chem. Soc.,* 2004, **126**, 16879; (b) M. Hu, J. S. Jiangand, Y. Zeng, *Chem. Commun.*, 2010, **46**, 1133; (c) M. Hu, A. A. Belik, H. Sukegawa, Y. Nemoto, M. Imura, Y. Yamauchi, *Chem. Asian J.*, 2011, **6**, 3195; (d) P. Dechambenoit, J. R. Long, *Chem .Soc. Rev.,* 2011, **40**, 3249; (e) M. Hu, A. A. Belik, M. Imura, K. Mibu, Y. Tsujimoto, Y. Yamauchi, *Chem. Mater.*, 2012, **24**, 2698.

6 D. Zhao, Q. Huo, J. Feng, B. F. Chmelka, G. D. Stucky, *J. Am. Chem. Soc.,* 1998, **120,** 6024.

7 (a) F. Fan, Z. Feng, C. Li, *Acc. Chem. Res.* 2010, **43**, 378; (b) J. Perez-Ramirez, F. Kapteijn, A. Bruckner, *J. Cal.* 2003, **218**, 234.

8 S. Zhu, D. Zhang, Z. Chen, Y. Zhang, *J. Mater. Chem.* 2009, **19**, 7710.

9 V. Blanco-Gutierrez, R. Saez-Puche, M. J. Torralvo-Fernandez, *J. Mater. Chem.,* 2012, **22**, 2992.

10 V. Blanco-Gutierrez, M. Virumbrales, R. Saez-Puche, M. J. Torralvo-Fernandez, *J. Phys. Chem. C*, 2013, **117**, 20927.

11 A. H. Morrish, *The Physical Principles of Magnetism*, Wiely IEEE Press., 2001.

12 E. P. Wohlfarth, in *Magnetism-Selected Topics*, ed. S. Foner. Gordon and Breach, New York, 1976, pp.1-59.

13 S. N. Kaul, A. Semwal, H. E. Schaefer, *Phys. Rev. B*., 2000, **62**, 13892.

14 S. Xuan, Yi-Xiang J. Wang, J. C. Yu and K. Cham-Fai Leung, *Chem. Mater.*, 2009, **21**, 5079.

This journal is © The Royal Society of Chemistry [year]

A table of contents

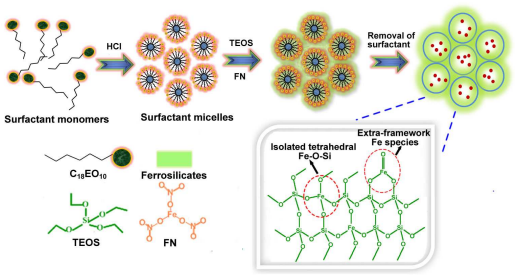

Ordered mesoporous ferrosilicate materials with highly dispersed iron oxide nanoparticles are directly synthesized through hydrothermal approach under acidic conditions.